

Original Article

Heterogeneous susceptibility for uraemic media calcification and concomitant inflammation within the arterial tree

Alexander H. Kirsch¹, Andrijana Kirsch², Katharina Artinger¹, Corinna Schabhüttl³, Walter Goessler⁴, Ingeborg Klymiuk⁵, Christian Güllý⁵, Gerald A. Fritz⁶, Saša Frank², Roxana Wimmer¹, Marianne Brodmann³, Hans-Joachim Anders⁷, Peter P. Pramstaller⁸, Alexander R. Rosenkranz¹, Kathrin Eller¹ and Philipp Eller^{3,9}

¹Department of Internal Medicine, Clinical Division of Nephrology, Medical University of Graz, Graz, Austria, ²Center of Molecular Medicine, Institute of Molecular Biology and Biochemistry, Medical University of Graz, Graz, Austria, ³Department of Internal Medicine, Division of Angiology, Medical University of Graz, Graz, Austria, ⁴Institute of Chemistry-Analytical Chemistry, Karl-Franzens University of Graz, Graz, Austria, ⁵Center for Medical Research, Core Facility Molecular Biology, Medical University of Graz, Graz, Austria, ⁶Department of Radiology, Medical University of Graz, Graz, Austria, ⁷Renal Division, Medizinische Klinik und Poliklinik IV, Klinikum der Universität München-Innenstadt, Munich, Germany, ⁸Center for Biomedicine, European Academy of Bolzano/Bozen, Bozen, Italy and ⁹Department of Internal Medicine, Intensive Care Unit, Medical University of Graz, Graz, Austria

Correspondence and offprint requests to: Philipp Eller; E-mail: philipp.eller@medunigraz.at

ABSTRACT

Background. End-stage renal disease (ESRD) is strongly associated with arterial calcification of the *tunica media*, decreased vascular compliance and sudden cardiac death. Here, we analysed the distribution pattern of uraemic media calcification and concomitant inflammation in mice and men.

Methods. Uraemia was induced in DBA/2 mice with high-phosphate diet. Subsequently, we analysed arterial medial calcification using histology, mass spectrometry, and wire myography. Gene expression was quantified using a whole transcriptome array and quantitative PCR. In a cohort of 36 consecutive patients with CKD stage 4–5, we measured the calcium score of the coronary arteries, the ascending thoracic aorta and the infrarenal abdominal aorta using computed tomography scans.

Results. Uraemic DBA/2 mice showed only minor calcifications in thoracic aortas, whereas there was overt media calcification in abdominal aortas. The transcriptional profile and immunohistochemistry revealed induction of Vcam1 expression by vascular smooth muscle cells in uraemic abdominal aortas. Macrophages infiltrated the tunica media of the abdominal

aorta. Anti-inflammatory treatment did not improve uraemic media calcification in our animal model. Arterial calcifications in ESRD patients showed a similar distribution pattern in computed tomography scans, with higher calcium scores of the abdominal aorta when compared with the thoracic aorta.

Conclusion. Taken together, there was a similar heterogeneous pattern of calcification in both mice and humans, where the abdominal aorta was more prone to media calcification when compared with the thoracic aorta. In uraemia, smooth muscle cells of the abdominal aorta showed a phenotypic switch to an inflammatory and osteoblastic phenotype.

Keywords: atherosclerosis, coronary calcification, ESRD, inflammation, vascular calcification

INTRODUCTION

Patients with chronic kidney disease (CKD) have a significantly increased cardiovascular morbidity and overall mortality [1]. Especially, patients suffering from end-stage renal disease (ESRD) have a 10- to 100-fold increased risk for cardiovascular morbidity and mortality compared with patients with normal kidney function [2, 3]. Thus, a 25-year-old patient on dialysis has a cardiovascular disease risk comparable to a 75-year-old

with intact renal function [1, 4]. This massive burden of cardiovascular disease in CKD and ESRD is strongly associated with extensive arterial calcifications, a reduced vascular compliance, left ventricular hypertrophy and sudden cardiac death [4]. As opposed to non-uraemic subjects where arterial calcification is a late occurrence and typically affects intimal atherosclerotic plaques, patients with CKD predominantly develop a calcification of the *tunica media*, which is most pronounced in the smooth muscle layers of large and medium-sized arteries [5]. Thus, uraemic media calcification and atherosclerotic intima calcification are distinct pathological entities with distinct spatiotemporal predilection sites [5].

Media calcification does not only occur in patients suffering from CKD and secondary hyperparathyroidism, but also in diabetics. Mönckeberg's media sclerosis is the prototype of media calcification. It is a common complication of long-standing diabetes mellitus, typically spares the *tunica intima* and has clear predilection for peripheral arteries. Although the first description dates back more than a century, many aspects of the precise pathogenesis of media calcification still remain unclear [6–8]. Hyperglycaemia and disturbances in calcium and phosphorus metabolism are established triggers of media calcification. Indeed, patients with advanced CKD and ESRD commonly show higher levels of serum phosphate and increased total body calcium content [2, 9].

Uraemic media calcification is not only driven by systemic factors such as hyperphosphatemia, low levels of calcification inhibitors or hyperglycaemia, but is also critically dependent on vascular smooth muscle cells (VSMC) per se. VSMC are not terminally differentiated cells, and in this manner they can eventually react to stress or injury by transdifferentiating from contractile to proliferative, osteoblastic and/or inflammatory phenotypes [10, 11]. Moreover, nascent VSMC derive from multiple, non-overlapping embryonic origins that are reflected in different anatomical locations within the adult and lead to a heterogeneous VSMC mosaic pattern. Ectodermal neuronal-crest derived VSMC populate the *tunica media* of the ascending thoracic aorta and the aortic arch, whereas the VSMC of the abdominal aorta are of mesenchymal origin [12, 13].

Finally, there is compelling evidence for inflammation in atherosclerosis at both the experimental and clinical level [14], whereas the role of inflammation in media calcification is still unclear. Recent immunohistochemical analyses found media calcification to be paralleled by significant higher *in situ* expression of proinflammatory markers (C-reactive protein, CD40 and CD154) in patients with CKD [5]. Therefore, we designed experiments and a clinical study to analyse distribution pattern and pathogenesis of uraemic media calcification in detail.

MATERIALS AND METHODS

Study design

Female 8-week-old dilute-brown agouti 2 (DBA/2NCrI, hereafter referred to as DBA/2) mice were obtained from Charles River (Sulzfeld, Germany) and housed in a virus/

antibody-free environment. These mice have an inherent susceptibility to high-phosphate diet-triggered calcification [15, 16]. To induce media calcification, they were placed on high-phosphate diet (Altromin, Germany) containing 20.2 g phosphorus, 9.4 g calcium, 0.7 g magnesium and 500 IU vitamin D3 per kg. The standard chow contained 7.0 g phosphorus, 10.0 g calcium, 2.2 g magnesium and 1000 IU vitamin D3 per kg. Mice were then followed for 5–14 days and culled under anaesthesia. For the interventional studies, DBA/2 mice were divided into three treatment groups to receive vehicle control (dimethylsulphoxide; Sigma, St. Louis, MO), TNF α inhibitor etanercept (Pfizer, New York, NY) at a dose of 10 mg/kg body weight, or TNF α receptor antagonist R-7050 (Santa Cruz, Dallas, TX) at a dose of 6 mg/kg body weight, respectively [17]. These drugs were applied via intraperitoneal injections every alternate day. All animal experiments were approved by Austrian veterinary authorities (BMWF-66.010/0047-II/3b/2012) and corresponded to directive 2010/63/EU of the European Parliament.

Histopathological, chemical and functional evaluation of media calcification

Aortas of DBA/2N mice were isolated and conserved for paraffin- as well as cryo-embedding. The extent of media calcification was determined histologically using Alizarin Red technique [18]. Alizarin Red staining was performed by incubating rehydrated paraffin sections in 2% Alizarin Red S solution (Sigma Aldrich, USA) followed by rinsing in acetone and acetone xylene. Expression of Vcam1, CD68 and Ly6G on vascular-smooth muscle, endothelial cells and infiltrating leucocytes, respectively, was assessed with standard immunohistochemical approaches, as previously described by our group [19].

Aortic mineral deposition was quantified in aortic samples using inductively coupled plasma mass spectrometry, as previously published by our group [20]. Briefly, the freeze-dried aortic samples were digested with nitric acid in a microwave-heated autoclave (UltraCLAVE III, EMLS, Leutkirch, Germany). The temperature was ramped in 45 min to 250°C and kept at this temperature for 45 min. After cooling, the samples were transferred to 50 mL polypropylene tubes. The calcium, phosphorus and magnesium concentrations were determined with an inductively coupled plasma mass spectrometry (Agilent 7500ce, Agilent Technologies, Waldbronn, Germany) at a mass-to-charge ratio of 43 for calcium, and 31 for phosphorus. The accuracy of the results was validated with the reference material bovine muscle (RM8414, NIST, Gaithersburg, ML, USA).

Functional evaluation of vascular compliance was done by wire. Aortic rings ~2 mm in length were cut from the thoracic aorta and abdominal aorta, respectively [21]. The rings were positioned in small wire myograph chambers (Danish Myo-Technology, Aarhus, Denmark), which contained physiological salt solution (PSS) (114 mM NaCl, 4.7 mM KCl, 0.8 mM KH₂PO₄, 1.2 mM MgCl₂, 2.5 mM CaCl₂, 25 mM NaHCO₃ and 11 mM D-glucose pH 7.4) aerated with 5% CO₂/95% O₂ at 37°C. The myograph chambers were connected to force transducers for isometric tension recording (PowerLab, ADInstruments, Spechbach, Germany). The rings were heated in PSS buffer to

37°C. An initial preload of 5 mN (abdominal rings) and 10 mN (thoracic rings) was then applied, and the rings were allowed to stabilize for 30 min. PSS containing 60 mM KCl (KPSS) was used to determine maximum contractility of the tissue. When the developed tension attained its peak value, the rings were relaxed by rinsing with the PSS buffer. Both, chemical and functional data were obtained each from two independent experiments.

Biochemical and molecular genetic evaluations

Biochemical analysis included serum electrolytes and serum urea (Roche, Mannheim, Germany). Total RNA was isolated from thoroughly cleaned murine aortic tissue using the RNeasy Mini Kit (Qiagen, the Netherlands) adhering to the manufacturer's instruction. Only RNA samples of RNA Integrity numbers >8.0 were used for further processing. Affymetrix GeneChip Mouse Gene Arrays 2.0ST (Affymetrix, Santa Clara, CA) were used with the Nugen Applause WT-Amp Plus ST System and the Encore Biotin Module (NuGEN Technologies, San Carlos, CA), GeneChip Eukaryotic Poly-A RNA Controls, hybridization Controls and the GeneChip Hybridization, Wash and Stain Kit (Affymetrix) according to the manufacturer's instruction. Arrays were scanned with the GeneChip Scanner GCS3000_7G. For generation of probe set expression values, CEL files containing probe level data were normalized using the robust multi-chip average algorithm implemented in the Partek Genomics Suite v6.6 Software (Partek, St Louis, MO). Subsequently, the data were log₂-transformed. Differences among groups are tested with analysis of variance (ANOVA) or *t*-tests using the appropriate contrasts. As criterion for filtering strongly regulated genes, a minimum fold change difference of at least 1.5-fold (up- or down-regulated) and significance at the level of $P \leq 0.05$ were used. Microarray data have been deposited in Gene Expression Omnibus (<http://www.ncbi.nlm.nih.gov/geo/>, accession number GSE57818). In order to confirm data of arrays, we performed qPCR experiments. Briefly, 2 µg of total RNA was reverse-transcribed using Superscript III Transcription Kit (Invitrogen) and random primers (Roche). Real-time PCR was performed in duplicates on a CF96 real-time detection system (BioRad, Vienna, Austria). For quantification of *Trp53inp1*, *Igfbp3*, *Casq1*, *Mtmr14*, *Col3a1*, *Coll1a1*, *Tnfa*, *Il1a* and *Vcam1* the gene expression assays Mm00458142_g1, Mm01187817_m1, Mm00486725_m1, Mm01184733_m1, Mm01254476_m1, Mm00801666_g1, Mm00443258_m1, Mm01336164_m1 and Mm01320970_m1 and TaqMan gene expression master mix (Life Technologies, Vienna, Austria) were used, respectively. *Hprt*, which served as housekeeping gene, and *Runx2* gene expression levels were assessed using SYBR green (BioRad) and the following primers: *Hprt* forward 5'-GCTTCTCCTCAGACCGTTTTTGC-3'; *Hprt* reverse 5'-ATCGCTAATCACGACGCTGGGACTG-3'; *Runx2* forward 5'-TCCTATCTGAGCCAGATGACATCC-3'; *Runx2* reverse 5'-CCGGTCTCCCCGGGTACC-3'.

Study population and computed tomography

We retrospectively enrolled 36 consecutive patients with CKD Stages 4–5 at the Clinical Division of Nephrology in Graz who underwent routine evaluations prior to kidney

transplantation between 2010 and 2014. The study protocol was approved by the Institutional Review Board of the Medical University of Graz (26_052 ex 13/14), and complied with the Declaration of Helsinki. The computed tomography (CT) examinations of heart and pelvis were routinely performed on a Toshiba Aquilion One 320-row detector CT scanner (Toshiba Medical Systems, Minato, Japan). The calcium score for the coronary arteries, the ascending thoracic aorta and the infrarenal abdominal aorta with the common iliac arteries was calculated by multiplying the calcification areas in mm² by a density score determined from the peak CT scan number (Agatston score) [22, 23] with a dedicated software (Vitrea, Toshiba Medical Systems) on a computed workstation by two independent experienced reviewers. Scores were determined for each main epicardial coronary artery, and the total calcium score was defined as the sum of the values of all lesions identified.

Statistical analysis

For large-scale gene function analysis, the Panther classification system was used according to Mi *et al.* [24]. Genes differentially regulated during diet interventions between the abdominal and thoracic aorta of FC > 0.3 with a P-value of at least 0.05 were used for pathway analysis using the Bonferroni correction.

Normal distribution of the data was assessed by the Kolmogorov–Smirnov test with Lilliefors correction. Calcification data in CKD patients was tested and analysed using ANOVA with subsequent Dunn's test with adjustment for multiple comparisons. Differences between the two groups were compared by either non-parametric Mann–Whitney *U*-test or unpaired Student's *t*-test as appropriate depending on the distribution of the tested variable. Intra- and inter-observer variability was assessed using Spearman's correlation. To assess intra-observer variability, each reader evaluated all datasets twice after a minimum delay of 1 month. A value of $P < 0.05$ was considered significant. Statistical analysis was done with GraphPad Prism 6.0 (GraphPad, La Jolla, CA).

RESULTS

High-phosphate diet induces media calcification in the abdominal aorta of DBA/2 mice

DBA/2 mice develop nephrocalcinosis and renal failure when put on high-phosphate diet [20], and uraemic DBA/2 mice are prone to develop media calcification after uninephrectomy [25]. In the first step, we established whether the acute onset of renal impairment together with the high dietary phosphate uptake was sufficient to induce uraemic media calcification in DBA/2 mice even in the absence of previous uninephrectomy. In the second step we analysed its distribution pattern. DBA/2 mice fed a high-phosphate diet over 5 days developed uraemia with significantly increased serum urea levels (197 ± 24 versus 53 ± 5 mg/dL; $n = 5$; $P = 0.001$) and significantly increased serum phosphate levels (18.6 ± 1.5 versus 13.3 ± 0.4 mmol/L; $n = 5$; $P = 0.02$) when compared with controls on standard chow, respectively. DBA/2 mice fed a high-phosphate diet for 14 days showed no histopathological signs of arterial calcifications in the ascending thoracic aorta and aortic arch

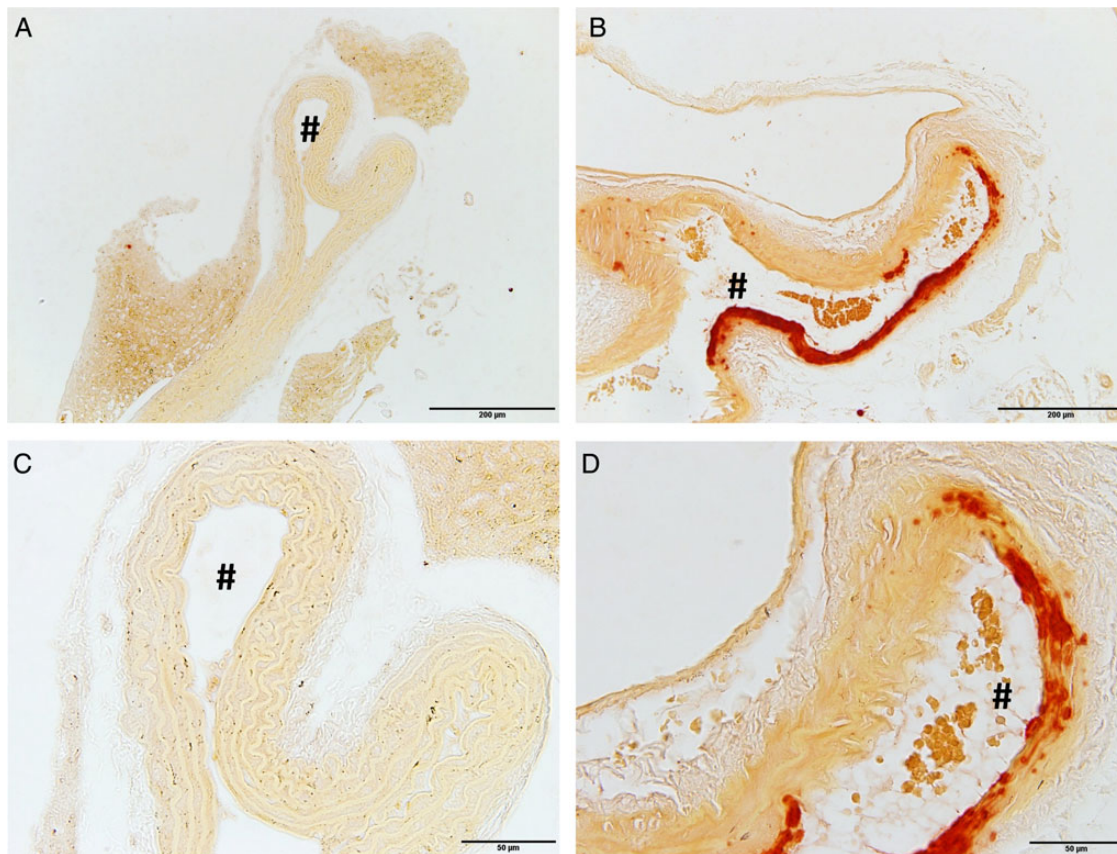


FIGURE 1: High-phosphate diet induces media calcification in the abdominal aorta, but not in the thoracic aorta. DBA/2 mice fed with a high-phosphate diet for 14 days developed no histopathological signs of arterial calcifications in the thoracic aorta (A and C), whereas there was a clear phenotype of media calcification in the abdominal aorta (B and D). The histopathological evaluation was performed with Alizarin Red stainings. # denotes the aortic lumen. The scale bar measures 200 μm (A, B) and 50 μm (C, D).

(Figure 1A and C), whereas there was a clear phenotype of vascular calcification in the abdominal aorta (Figure 1B and D). This arterial calcification did not occur in atherosclerotic plaques of the *Tunica intima*, but was most pronounced in the VSMC of the *Tunica media*. Age-matched controls on standard chow did not develop any media calcification (data not shown).

Next, we independently confirmed this distribution pattern of media calcification by chemical analyses of mineral precipitation in the diverse aortic segments using inductively coupled plasma mass spectrometry. Both, the abdominal and the thoracic aorta displayed higher amounts of phosphorus content in animals fed with high-phosphate diet, when compared with mice on standard chow (Figure 2A and B). Moreover, abdominal aortic tissue of DBA/2 mice on phosphorus-rich diet displayed a significantly higher calcium (29.4 ± 10.1 versus 5.1 ± 1.8 $\mu\text{g}/\text{mg}$ dry weight; $n = 10$; $P < 0.05$) and phosphorus content (18.8 ± 4.1 versus 7.4 ± 0.4 $\mu\text{g}/\text{mg}$ dry weight; $n = 10$; $P < 0.05$) when compared with the thoracic segments (Figure 2A and B). Of note, there was no difference in the mineral content of thoracic and abdominal aortic segments of standard-chow fed mice. Interestingly, we also found a significantly higher mineral content of magnesium within the aortic wall of DBA/2 mice treated with a high-phosphate diet (Figure 2A and B), whereas there was no difference in the serum concentration of magnesium between DBA/2 mice on high-phosphate diet and control mice on

standard chow (0.92 ± 0.07 mmol/L versus 0.91 ± 0.02 mmol/L; $n = 5$ per group; $P = 0.86$).

Media calcification impairs VSMC contractility and changes the vascular compliance. Therefore, we performed wire myography experiments in order to quantify the functional impact of media calcification on the aorta. Wire myography measurements in DBA/2 mice on standard chow showed a similar maximum contraction upon challenge with 60 mM KCl in the thoracic and abdominal aorta, respectively (Figure 2C and D). In sharp contrast, DBA/2 mice on high-phosphate diet had a significantly impaired maximum contraction of their abdominal aorta ($P < 0.001$), whereas there was no change in contractility of the thoracic aorta (Figure 2C and D). Thus, histological, chemical and functional analyses consistently showed a pattern of uraemic media calcification in DBA/2 mice, which was prominent in the abdominal aorta and spared the ascending thoracic aorta and the aortic arch.

Media calcification is associated with induction of an inflammatory VSMC phenotype in the abdominal aorta

Next, we investigated the molecular basis of this heterogeneous susceptibility for media calcification and determined the entire transcriptional profile of both the abdominal and thoracic aorta upon high-phosphate diet and standard chow, respectively. Hierarchical cluster analysis of these array data

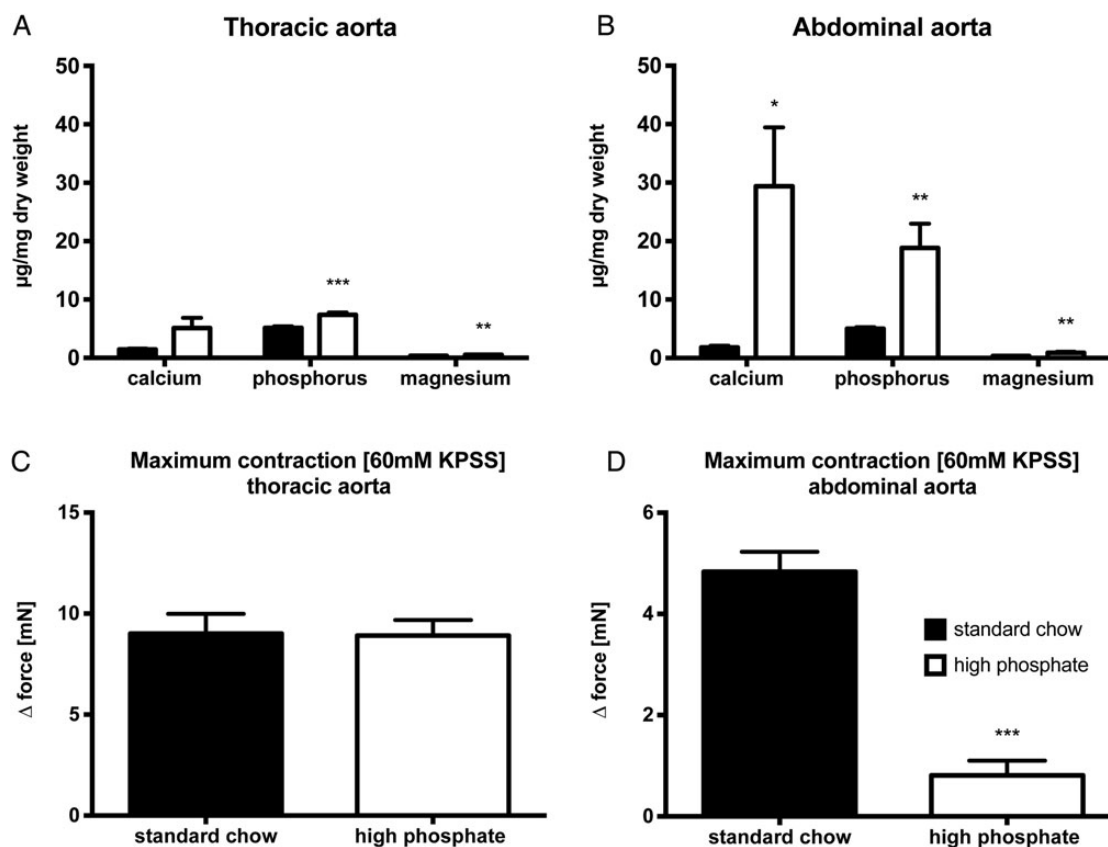


FIGURE 2: Chemical and functional evaluation of aortic media calcification. Mineral content was chemically measured by inductively coupled plasma mass spectrometry in the thoracic (A) and abdominal aorta (B) after 14 days on high-phosphate diet (white bars) or standard chow (black bars) ($n = 10$ in each group). The functional impact of this media calcification on vascular contractility was evaluated by wire myography in thoracic (C; $n = 7$ in each group), and abdominal aortic segments (D, $n = 15$ in each group) after 9 days on high-phosphate diet (white bars) or standard chow (black bars), respectively. * indicates a P-value <0.05 , ** indicates a P-value <0.01 and *** indicates a P-value <0.001 .

indicated that gene transcription in aortic tissue samples was primarily determined by anatomical location. Exposure to high-phosphate diet was a subordinate hierarchy element in VSMC phenotypic modulation (Figure 3). This observation infers that there is a clear positional identity of VSMC in the thoracic and abdominal aorta, which is a stronger determinant of gene expression than the influence of the hyperphosphatemic and uraemic milieu. After 5 days on high-phosphate diet, VSMC of the abdominal aorta showed an upregulation of, e.g. vascular cell adhesion molecule-1 *Vcam1*, which is a typical marker of inflammatory VSMC phenotype [26]. These array data were independently reproduced in real-time PCR experiments (Figure 4A and B). Moreover, immunohistochemical stainings confirmed that the increased *Vcam1* expression was clearly localized in the medial arterial wall and not in the endothelium (Figure 4E and F). The induction of an inflammatory VSMC phenotype in the abdominal aorta was associated with a significantly higher expression of the osteoblastic marker *Runx2* after 14 days on high-phosphate diet and a parallel repression of the contractile and synthetic VSMC phenotype as exemplified by downregulation of caldesmon-1 *Casq1* and collagen type III α 1 and type I α 1 isoforms *Col3a1* and *Col1a1*, respectively (Figure 4B and D). *Vcam1* expression was associated with an infiltration of CD68+ macrophages that

accumulated within the *tunica media* around vascular calcifications after 14 days of treatment with high-phosphate diet (Figure 5A), and was paralleled by a sparse infiltration of Ly6G+ neutrophil granulocytes in the *tunica adventitia* of the abdominal aorta (Figure 5B). No relevant CD4+ or CD8+ T cells were detectable at this time point neither in the *adventitia* nor in the *tunica media* (data not shown). To further analyse the role of vascular inflammation in media calcification, we exposed DBA/2 mice on high-phosphate diet first to the TNF α inhibitor etanercept and then to the TNF α receptor antagonist R-7050. We decided to block TNF α and its signalling since it is central in T cell and macrophage immune mediation [27] and its blockade was successful in decreasing atherosclerosis in ApoE knock-out mice [28]. However, TNF α inhibitor treatment did not influence survival of mice (Figure 6A) and both therapeutic interventions did not decrease the amount of abdominal aortic media calcification in our experimental setting (Figure 6B and C). Interestingly, both treatment options rather increased the amounts of phosphate in the abdominal aorta, which reached significance in mice treated with the TNF α receptor antagonist R-7050 (Figure 6B and C). Of note, both treatments did not alter kidney calcification and kidney function measured by serum urea and lipocalin 2 (data not shown).

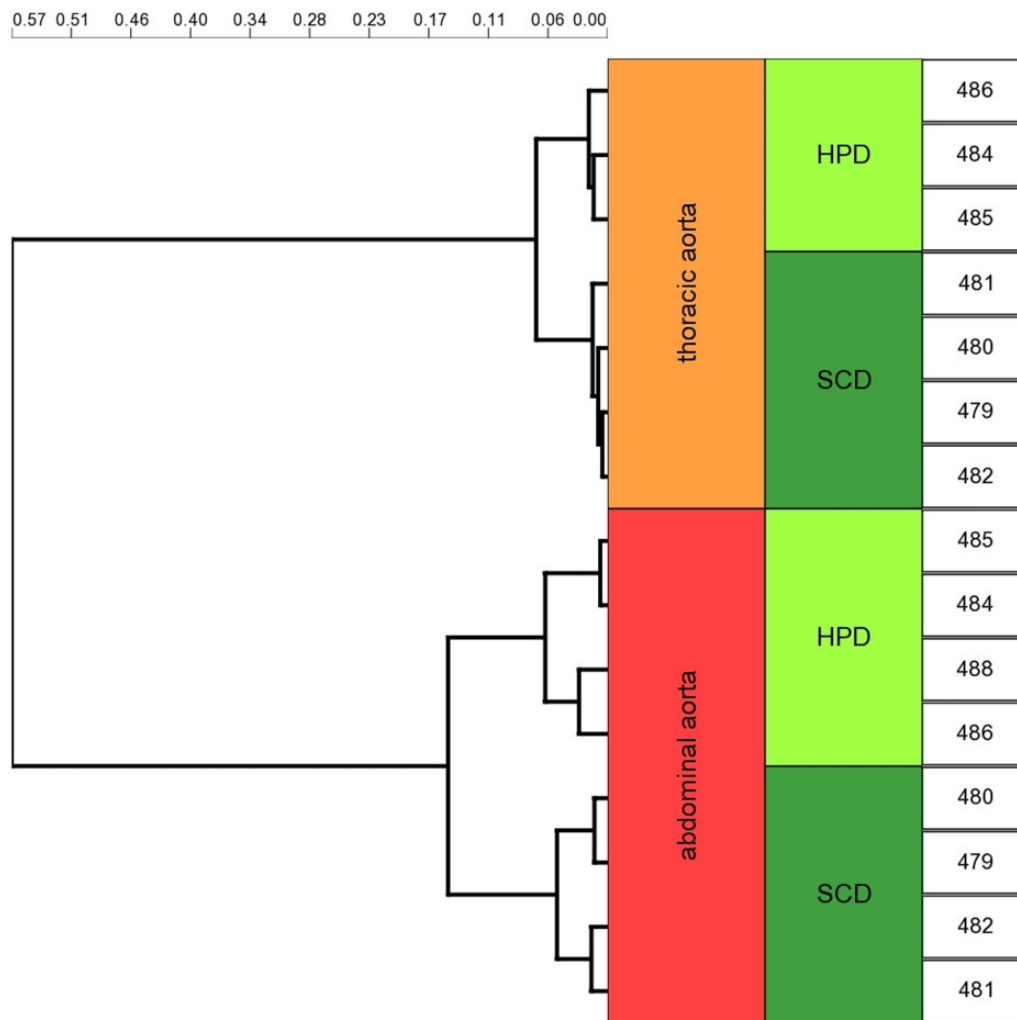


FIGURE 3: Hierarchical cluster analysis of Affimetrix mouse gene 2.0 ST arrays of thoracic and abdominal aorta of DBA/2 mice fed with standard chow diet or high-phosphate diet. Cluster analysis on pairwise Pearson's dissimilarity of the whole transcriptome using the Ward's method revealed two prominent clusters in the dendrogram that primarily reflected the anatomical location of the tissue sample. Exposure to high-phosphate diet (HPD) or standard chow diet (SCD) was a subordinate hierarchy element in this clustering analysis. Genomic data were deposited in the NCBI gene expression and hybridization array data repository (GEO) under the GEO accession number GSE57818.

Distribution pattern of media calcification in patients suffering from ESRD

In order to investigate these findings of a heterogeneous susceptibility for uraemic media calcification in the clinical setting, we conducted a retrospective cohort study of patients suffering from ESRD, who routinely underwent CT scans of the heart and the pelvis prior to kidney transplantation (Figure 7A–C). The clinical and biochemical characteristics of our study population are given in Table 1. We calculated the calcium scores for the coronary arteries, the ascending thoracic aorta with the aortic arch and the infrarenal abdominal aorta with the common iliac arteries, which each derive from different embryonic origins: the proepicardium, the neuronal crest and the splanchnic mesoderm, respectively [12]. As shown in Figure 7D, the degree of media calcification in the infrarenal abdominal aorta, iliac and coronary arteries was significantly higher when compared with the ascending thoracic aorta. Thus, there was a similar heterogeneous pattern of uraemic media calcification in both mice and humans, where mesenchyme-derived arteries are

more prone to media sclerosis and media calcification when compared with neuronal-crest derived arteries such as the ascending thoracic aorta and the aortic arch. The intra- and inter-observer agreement of calcium scores was excellent in our dataset ($r > 0.997$).

DISCUSSION

Uraemic media calcification is strongly associated with cardiovascular mortality in CKD patients, but so far detailed information on its pathogenesis as well as therapeutic options are limited. Here, we show that uraemic media calcification differs from atherosclerosis in its spatiotemporal predilection sites and that it is paralleled by local vascular inflammation in its early phase.

In animal studies, different genetic backgrounds of inbred strains modulate the occurrence and degree of vascular calcifications [29, 30]. C57Bl/6 mice are resistant to vascular calcifications [30], whereas Fetuin-A and Matrix Gla protein-deficient

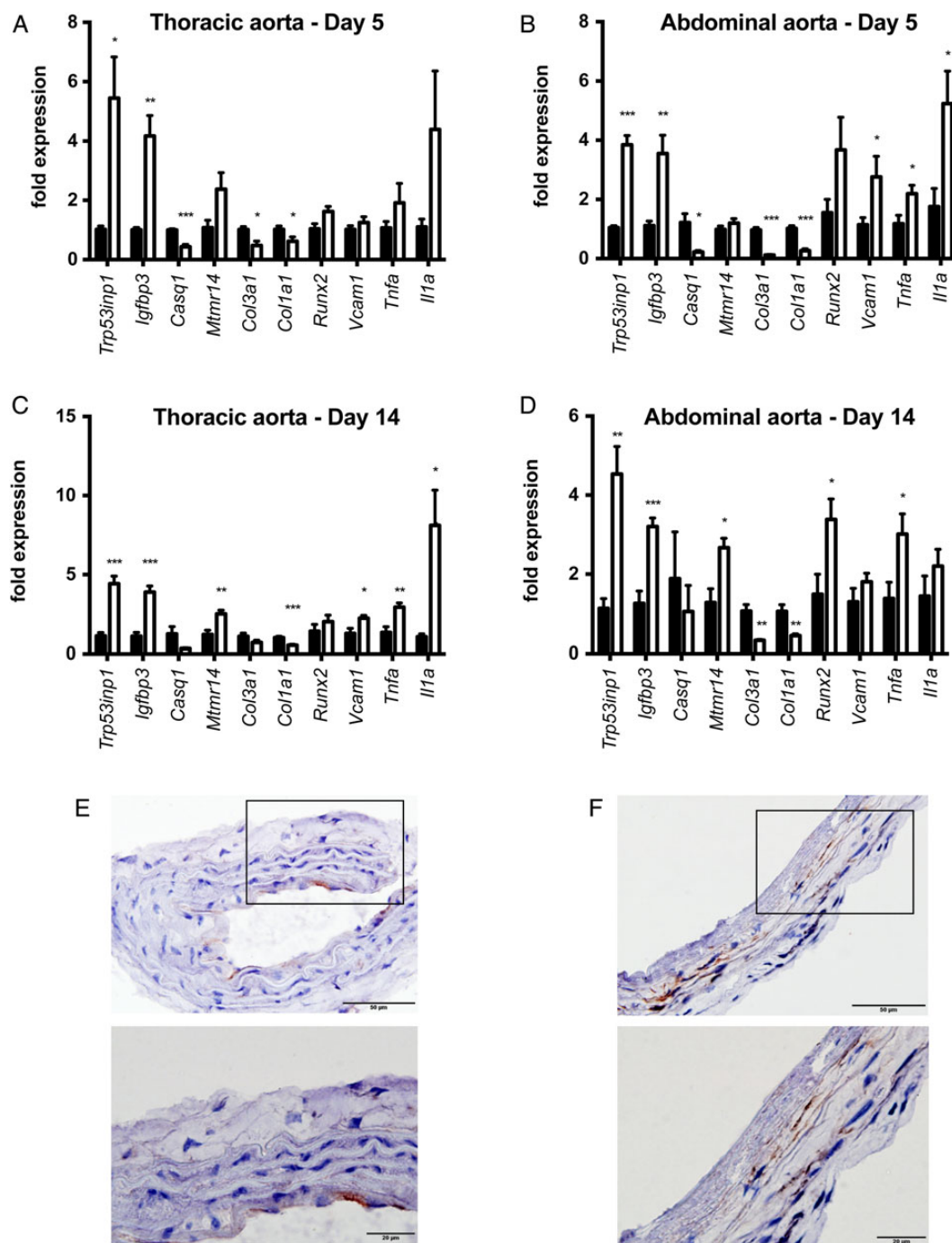


FIGURE 4: Media calcification is associated with an inflammatory and osteoblastic vascular smooth muscle cell phenotype in the abdominal aorta. DBA/2 mice were fed with high-phosphate diet (white bars) or standard chow (black bars) for 5 (A and B) or 14 days (C and D), respectively ($n = 4$ in each group). Quantitative PCR analyses of thoracic (A and C) and abdominal aorta (B and D) revealed a repression of the contractile and synthetic VSMC phenotype and a parallel induction of an inflammatory and osteoblastic VSMC phenotype that was more pronounced in the abdominal aorta. The *Vcam1* expression in the abdominal aorta (B) was also seen in immunohistochemistry experiments, where there was a positive signal in the *Tunica media* (F), while *Vcam1* expression in the thoracic aorta was restricted to the endothelium (E). The scale bar measures 50 μm (top row) and 20 μm (bottom row).

mice develop early calcifications in the aortic arch [31, 32]. Contrary to these animal models without kidney disease, but similarly to data by El-Abbadi *et al.* [25] media calcification was more prominent in the abdominal aorta when compared with the thoracic aorta in our uraemic DBA/2 mice. Although exposed to the same soluble factors and morphogenetic cues

upon high-phosphate diet, the VSMC of the abdominal aorta in DBA/2 mice were more prone to switch to an inflammatory/osteoblastic phenotype and to calcify when compared with the ascending thoracic aorta and the aortic arch. Our clinical study in patients with end-stage renal failure independently reproduced these preclinical data revealing significantly higher

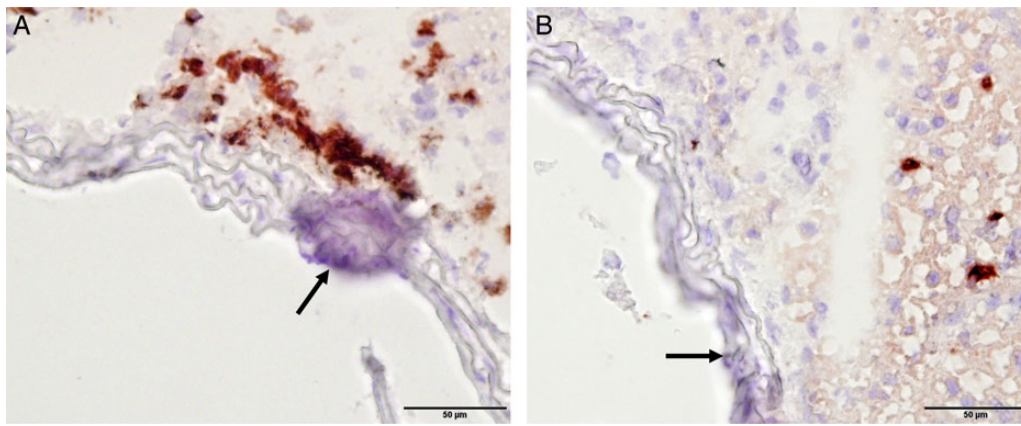


FIGURE 5: Infiltration of macrophages near foci of media calcification in the abdominal aorta. Immunohistochemical staining of CD68+ macrophages (A) and Ly6G+ neutrophil granulocytes (B) in abdominal aortas of DBA/2 mice after 14 days of treatment with high-phosphate diet. Macrophages accumulated in the Tunica adventitia and infiltrated the Tunica media around established foci of media calcification (arrow).

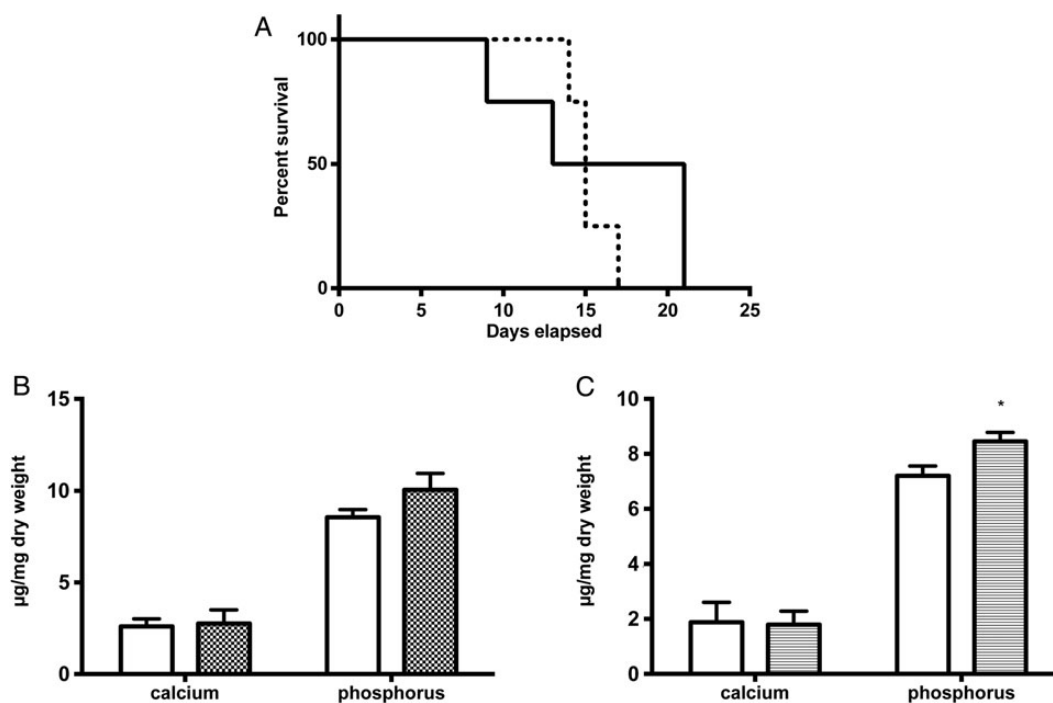


FIGURE 6: Treatment with a TNF α inhibitor as well as a TNF α receptor antagonist does not influence survival and did not inhibit media calcification of the abdominal aorta. DBA/2 mice were fed with a high-phosphate diet and were treated with the TNF α inhibitor etanercept (dashed line) or vehicle (solid line) and followed for survival (A; $n = 4$ per group). Mice treated with the TNF α inhibitor etanercept (B; grey bar; $n = 4$) or the TNF α receptor antagonist R-7050 (C; grey bar; $n = 4$) were analysed for calcification of the abdominal aorta and compared with vehicle-treated mice (white bars) after 10 days of high-phosphate diet. Data are given as means \pm SEM.

calcium scores of the infrarenal abdominal aorta, iliac and coronary arteries when compared with the ascending thoracic aorta and aortic arch. Of note, we have previously detected a similar heterogeneous distribution pattern of vascular calcification in a small cohort of patients suffering from ESRD, although this previous clinical study was not designed to specifically address this issue [23]. The primary clinical consequence of this finding is that ESRD patients with a high calcium score of the coronary arteries should be screened for extensive uraemic media calcification of the iliac arteries before planning kidney transplantation with arterial anastomoses to the iliac arteries.

Vice versa, a low degree of calcification of the ascending aorta in CT scans does not necessarily imply a low level of uraemic media calcification of the abdominal aorta and/or iliac arteries. Thus, transplantation surgeons may anticipate perioperative complications when taking into account that there is a heterogeneous pattern of uraemic media calcification in ESRD patients.

The different inherent susceptibilities to uraemic media calcification within the arterial tree seem to correlate with the distinct embryological origins of the VSMC layer within the arterial tree [12]. VSMC of mesenchyme-derived arteries

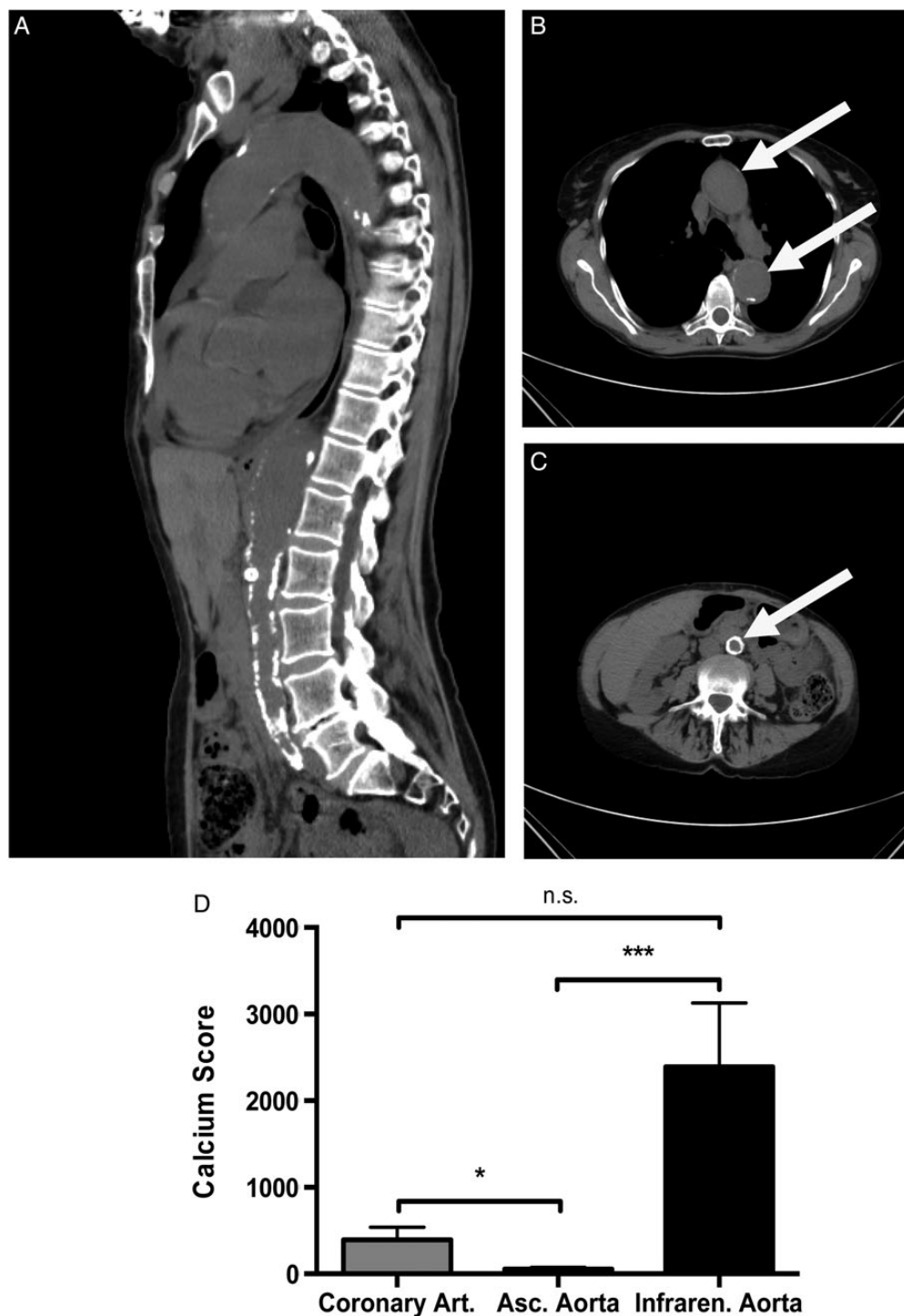


FIGURE 7: Uraemic media calcification in patients with chronic kidney disease. Representative CT images with a sagittal reconstruction (A) and a transverse section of the thoracic (B) and abdominal aorta (C) are shown in a patient with chronic kidney disease Stage IV (estimated glomerular filtration rate of 28 mL/min/m²) due to hypertensive nephropathy. The white arrow indicates the position of the aorta. (D) In a cohort of 36 in patients with end-stage renal failure, the calcium scores of the ascending aorta (white bar), the coronary (grey bar) and infrarenal aorta with the common iliac arteries (black bar) were measured by native CT scans. The calcium score of the ascending thoracic aorta was significantly lower, when compared with the calcium scores of the abdominal aorta or coronary arteries, respectively. Data are given as means \pm SEM. n.s., not significant. * indicates a P-value <0.05, *** indicates a P-value <0.001.

such as the abdominal aorta and coronary arteries are more prone to transdifferentiate into an inflammatory/osteoblastic phenotype when compared with VSMC cells of neuronal-crest derived arteries such as the ascending thoracic aorta and the

aortic arch. This peculiar facet constitutes a major difference of uraemic media calcification to the pathogenesis of atherosclerosis, where branching points of arteries with turbulent blood flow are classic predilection sites for primordial

Table 1. Characteristics of patients with chronic kidney disease

Gender (male/female)	23/13
Age (years)	49 ± 2
Dialysis vintage (months)	20 ± 4
Type of dialysis (haemodialysis/peritoneal dialysis)	21/15
Prior kidney transplantation (n;%)	8 (22.2%)
Body mass index (kg/m ²)	26.1 ± 0.8
Current smoking (n;%)	8 (22.2%)
Systolic blood pressure (mmHg)	136 ± 3
Diastolic blood pressure (mmHg)	84 ± 2
Creatinine (mg/dL)	7.7 ± 0.6
Albumin (g/L)	39.3 ± 1.3
Glycohemoglobin (mmol/mol)	32.4 ± 0.8
Total cholesterol (mg/dL)	185 ± 7
LDL cholesterol (mg/dL)	106 ± 6
HDL cholesterol (mg/dL)	51 ± 4
Triglycerides (mg/dL)	147 ± 14
C-reactive protein (mg/dL)	4.2 ± 0.7
Calcium (mmol/L)	2.29 ± 0.05
Phosphate (mmol/L)	1.66 ± 0.07
Parathyroid hormone (ng/L)	346 ± 37
Dose of oral calcium (g/year)	17.4 (0–34.7)
Calcitriol (n;%)	20 (55.6%)
Sevelamer (n;%)	14 (38.9%)
Aluminium hydroxide (n;%)	2 (5.6%)
Lanthanum carbonate (n;%)	2 (5.6%)
Cinacalcet (n;%)	8 (22.2%)
Statin (n;%)	8 (22.2%)

atherosclerotic plaques [14]. Our data parallel similar findings on origin-specific differences of VSMC growth control [33, 34], responses to vasoactive stimuli [35], and activation of cytokine signalling pathways [36, 37]. There is accumulating evidence that VSMC derived from different lineages exhibit morphologically and functionally distinct properties and respond differently to soluble factors and morphogenetic cues *in vivo* [38]. The underlying molecular mechanisms for the lineage-specific properties and the diverse phenotypes exhibited by VSMC seem to have evolved as adaptive survival mechanisms, and allow VSMC to repair damage after vascular injury or to adjust responses to changing hemodynamic demands [10]. Thus, VSMC have a positional identity in diverse arterial segments with important functional implications both during the development and during vascular disease [39].

Employing a genome-wide approach, we also found VSMC of the abdominal aorta, but not VSMC of the aortic arch to switch to an inflammatory and osteoblastic phenotype when exposed to uraemia. The phenotypic switch of VSMC was reflected by *Vcam1* upregulation in the *tunica media* and was paralleled by a repression of the contractile and synthetic VSMC phenotype as exemplified by downregulation of myoglobin, caldesmon-1 and collagen type III and I $\alpha 1$ isoforms, respectively. Immediately after vascular injury, there seems to be a downregulation of collagen type I expression, whereas at later time points in vascular repair there is an induction of collagen type I expression ultimately leading to fibrotic remodeling [40–42]. This phenotypic modulation of VSMC was accompanied by a sparse infiltration of immune cells of the innate immune system into the *tunica media*. Similar data were obtained by Amann K. who showed immune cells to infiltrate in the *tunica media* of patients with established media sclerosis [5]. We further chose to block TNF α and its signalling to

evaluate the role of inflammation in media sclerosis. We chose this approach since TNF α is central in T cell and macrophage immune mediation [27] and this strategy was successful in limiting atherosclerosis in ApoE knock-out mice [28]. Contrary to data in models of atherosclerosis, the interruption of TNF α signalling did not improve uraemic media calcification in our animal model. Interruption of TNF α signalling even increased phosphate contents in the vascular wall. In line with these data, T-cell modulation in DBA/2 mice did not change cardiac calcifications even though renal calcifications were improved [20]. Our findings also nicely concur with the clinical evidence showing that anti-inflammatory strategies such as statin therapy did not improve cardiovascular mortality in ESRD patients [14, 43, 44].

Together, these data highlight a distinct aspect of uraemic media calcification, and underline the need for further research on the molecular mechanisms underlying vascular calcification in order to relieve the cardiovascular burden of ESRD patients.

ACKNOWLEDGEMENTS

This work was supported by the Austrian Science Funds (FWF) to A.R.R. (P-21402) and to P.E. and K.E. (P27537), by the Paracelsus and Joseph Skoda Award of Austrian Society of Internal Medicine to E.P., respectively. A.H.K. is a recipient of a DOC Fellowship of the Austrian Academy of Sciences. A.H.K. and A.K. are enrolled in the PhD program in molecular medicine at the Medical University of Graz.

CONFLICT OF INTEREST STATEMENT

None declared.

REFERENCES

- Go AS, Chertow GM, Fan D *et al*. Chronic kidney disease and the risks of death, cardiovascular events, and hospitalization. *N Engl J Med* 2004; 351: 1296–1305
- Block GA, Klassen PS, Lazarus JM *et al*. Mineral metabolism, mortality, and morbidity in maintenance hemodialysis. *J Am Soc Nephrol* 2004; 15: 2208–2218
- Foley RN, Murray AM, Li S *et al*. Chronic kidney disease and the risk for cardiovascular disease, renal replacement, and death in the United States Medicare population, 1998 to 1999. *J Am Soc Nephrol* 2005; 16: 489–495
- Goodman WG, Goldin J, Kuizon BD *et al*. Coronary-artery calcification in young adults with end-stage renal disease who are undergoing dialysis. *N Engl J Med* 2000; 342: 1478–1483
- Amann K. Media calcification and intima calcification are distinct entities in chronic kidney disease. *Clin J Am Soc Nephrol* 2008; 3: 1599–1605
- Lanzer P, Boehm M, Sorribas V *et al*. Medial vascular calcification revisited: review and perspectives. *Eur Heart J* 2014; 35: 1515–1525
- Zoccali C, London G. Con: vascular calcification is a surrogate marker, but not the cause of ongoing vascular disease, and it is not a treatment target in chronic kidney disease. *Nephrol Dial Transplant* 2015; 30: 352–357
- Bover J, Evenepoel P, Ureña-Torres P *et al*. Pro: cardiovascular calcifications are clinically relevant. *Nephrol Dial Transplant* 2015; 30: 345–351
- McIntyre CW. Calcium balance during hemodialysis. *Semin Dial* 2008; 21: 38–42
- Owens GK, Kumar MS, Wamhoff BR. Molecular regulation of vascular smooth muscle cell differentiation in development and disease. *Physiol Rev* 2004; 84: 767–801

11. Proudfoot D, Skepper JN, Hegyi L *et al*. Apoptosis regulates human vascular calcification in vitro: evidence for initiation of vascular calcification by apoptotic bodies. *Circ Res* 2000; 87: 1055–1062
12. Majesky MW. Developmental basis of vascular smooth muscle diversity. *Arterioscler Thromb Vasc Biol* 2007; 27: 1248–1258
13. Hao H, Gabbiani G, Bochaton-Piallat M-L. Arterial smooth muscle cell heterogeneity: implications for atherosclerosis and restenosis development. *Arterioscler Thromb Vasc Biol* 2003; 23: 1510–1520
14. Libby P, Ridker PM, Maseri A. Inflammation and atherosclerosis. *Circulation* 2002; 105: 1135–1143
15. Meng H, Vera I, Che N *et al*. Identification of Abcc6 as the major causal gene for dystrophic cardiac calcification in mice through integrative genomics. *Proc Natl Acad Sci U S A* 2007; 104: 4530–4535
16. Jansen RS, Duijst S, Mahakena S *et al*. ATP-binding cassette subfamily C member 6-mediated ATP secretion by the liver is the main source of the mineralization inhibitor inorganic pyrophosphate in the systemic circulation. *Arterioscler Thromb Vasc Biol* 2014; 34: 1985–1989
17. Lech M, Gröbmayr R, Ryu M *et al*. Macrophage phenotype controls long-term AKI outcomes—kidney regeneration versus atrophy. *J Am Soc Nephrol* 2014; 25: 292–304
18. Eller P, Eller K, Kirsch AH *et al*. A murine model of phosphate nephropathy. *Am J Pathol* 2011; 178: 1999–2006
19. Eller K, Kirsch A, Wolf AM *et al*. Potential role of regulatory T cells in reversing obesity-linked insulin resistance and diabetic nephropathy. *Diabetes* 2011; 60: 2954–2962
20. Kirsch AH, Smaczny N, Riegelbauer V *et al*. Regulatory T cells improve nephrocalcinosis but not dystrophic cardiac calcinosis in DBA/2 mice. *Am J Pathol* 2013; 183: 382–390
21. Rao SP, Riederer M, Lechleitner M *et al*. Acyl chain-dependent effect of lysophosphatidylcholine on endothelium-dependent vasorelaxation. *PLoS One* 2013; 8: e65155
22. Agatston AS, Janowitz WR, Hildner FJ *et al*. Quantification of coronary artery calcium using ultrafast computed tomography. *J Am Coll Cardiol* 1990; 15: 827–832
23. Eller P, Hochegger K, Feuchtner GM *et al*. Impact of ENPP1 genotype on arterial calcification in patients with end-stage renal failure. *Nephrol Dial Transplant* 2008; 23: 321–327
24. Mi H, Muruganujan A, Casagrande JT *et al*. Large-scale gene function analysis with the PANTHER classification system. *Nat Protoc* 2013; 8: 1551–1566
25. El-Abadi MM, Pai AS, Leaf EM *et al*. Phosphate feeding induces arterial medial calcification in uremic mice: role of serum phosphorus, fibroblast growth factor-23, and osteopontin. *Kidney Int* 2009; 75: 1297–1307
26. Couffinhal T, Dupl a C, Moreau C *et al*. Regulation of vascular cell adhesion molecule-1 and intercellular adhesion molecule-1 in human vascular smooth muscle cells. *Circ Res* 1994; 74: 225–234
27. Watts TH. TNF/TNFR family members in costimulation of T cell responses. *Ann Rev Immunol* 2005; 23: 23–68
28. Br n n L, Hovgaard L, Nitulescu M *et al*. Inhibition of tumor necrosis factor- α reduces atherosclerosis in apolipoprotein E knockout mice. *Arterioscler Thromb Vasc Biol* 2004; 24: 2137–2142
29. Berndt A, Li Q, Potter CS *et al*. A single-nucleotide polymorphism in the Abcc6 gene associates with connective tissue mineralization in mice similar to targeted models for pseudoxanthoma elasticum. *J Invest Dermatol* 2013; 133: 833–836
30. Qiao JH, Xie PZ, Fishbein MC *et al*. Pathology of atheromatous lesions in inbred and genetically engineered mice. Genetic determination of arterial calcification. *Arterioscler Thromb* 1994; 14: 1480–1497
31. Westenfeld R, Sch fer C, Kr ger T *et al*. Fetuin-A protects against atherosclerotic calcification in CKD. *J Am Soc Nephrol* 2009; 20: 1264–1274
32. Leroux-Berger M, Queguiner I, Maciel TT *et al*. Pathologic calcification of adult vascular smooth muscle cells differs on their crest or mesodermal embryonic origin. *J Bone Miner Res* 2011; 26: 1543–1553
33. Cheung C, Bernardo AS, Trotter MWB *et al*. Generation of human vascular smooth muscle subtypes provides insight into embryological origin-dependent disease susceptibility. *Nat Biotechnol* 2012; 30: 165–173
34. Topouzis S, Majesky M. Smooth muscle lineage diversity in the chick embryo. *Dev Biol* 1996; 178: 430–445
35. Owens AP, Subramanian V, Moorleghen JJ *et al*. Angiotensin II induces a region-specific hyperplasia of the ascending aorta through regulation of inhibitor of differentiation 3. *Circ Res* 2010; 106: 611–619
36. Xie W-B, Li Z, Shi N *et al*. Smad2 and myocardin-related transcription factor B cooperatively regulate vascular smooth muscle differentiation from neural crest cells. *Circ Res* 2013; 113: e76–e86
37. Trigueros-Motos L, Gonz lez-Granado JM, Cheung C *et al*. Embryological-origin-dependent differences in homeobox expression in adult aorta: role in regional phenotypic variability and regulation of NF- κ B activity. *Arterioscler Thromb Vasc Biol* 2013; 33: 1248–1256
38. O'Neill WC, Adams AL. Breast arterial calcification in chronic kidney disease: absence of smooth muscle apoptosis and osteogenic transdifferentiation. *Kidney Int* 2014; 85: 668–676
39. Awgulewitsch A, Majesky MW. Interpreting inflammation: smooth muscle positional identity and nuclear factor- κ B signaling. *Arterioscler Thromb Vasc Biol* 2013; 33: 1113–1115
40. Weng X, Cheng X, Wu X *et al*. Sin3B mediates collagen type I gene repression by interferon gamma in vascular smooth muscle cells. *Biochem Biophys Res Commun* 2014; 447: 263–270
41. Blackstock CD, Higashi Y, Sukhanov S *et al*. Insulin-like growth factor-1 increases synthesis of collagen type I via induction of the mRNA-binding protein LARP6 expression and binding to the 5' stem-loop of COL1a1 and COL1a2 mRNA. *J Biol Chem* 2014; 289: 7264–7274
42. Simionescu A, Simionescu DT, Vyavahare NR. Osteogenic responses in fibroblasts activated by elastin degradation products and transforming growth factor- β 1: role of myofibroblasts in vascular calcification. *Am J Pathol* 2007; 171: 116–123
43. Wanner C, Krane V, M rz W *et al*. Atorvastatin in patients with type 2 diabetes mellitus undergoing hemodialysis. *N Engl J Med* 2005; 353: 238–248
44. Fellstr m BC, Jardine AG, Schmieder RE *et al*. Rosuvastatin and cardiovascular events in patients undergoing hemodialysis. *N Engl J Med* 2009; 360: 1395–1407

Received for publication: 28.2.2015; Accepted in revised form: 1.6.2015